Organic & Biomolecular Chemistry

ROYAL SOCIETY OF CHEMISTRY

PAPER

View Article Online
View Journal | View Issue

Cite this: *Org. Biomol. Chem.*, 2024, **22**, 1892

Fluorescent protein chromophores modified with aromatic heterocycles for photodynamic therapy and two-photon fluorescence imaging†

Weilong Li, Wan Feng, Badi Liu and Ying Qian *

In this paper, three fluorescent protein chromophore analogs PFPAr (PFPP, PFPC, and PFPT) were synthesized and proved to be useful for photodynamic therapy and two-photon fluorescence imaging. By adding five- or six-membered aromatic heterocycles to the photosensitizer PFP, we obtained three fluorescent protein photosensitizers PFPAr with better performances. As a demonstration, compared with the reported photosensitizer PFP, photosensitizer PFPP exhibits larger emission wavelengths (701 nm) and achieves a slight enhancement in the efficiency of singlet oxygen (Φ_Δ = 23%). Notably, PFPP can perform good two-photon fluorescence imaging with an 800 nm femtosecond laser in zebrafish. In *in vitro* cytotoxicity assays, PFPP shows good phototoxicity (IC_{50} = 4.12 μM) and acceptable dark toxicity (cell viability assay >90%). The reactive oxygen imaging experiments and AO/EB double staining assay indicate that PFPP can generate singlet oxygen to eliminate A-549 tumor cells effectively with photoexcitation of 460 nm blue light (20 mW cm^{-2}). Furthermore, PFPP can label the lysosomes of tumor cells with high specificity for lysosomes (Pearson's correlation coefficient of 0.91). Thus, our study demonstrated that the rational introduction of aromatic heterocycles into fluorescent protein photosensitizers can effectively enhance the key parameters of photosensitivity and pave the way for further two-photon photodynamic therapy.

Received 4th December 2023,
Accepted 1st February 2024

DOI: 10.1039/d3ob01966g

rsc.li/obc

1. Introduction

Green fluorescent protein (GFP) has been extensively studied due to its advantageous properties,[1,2] including good biocompatibility, unique fluorescence properties, and large Stokes shift.[3–5] 4-Hydroxybenzylidene imidazolidinone (HBI) is the fluorescent core of GFP, which is often used as a modification center for synthesizing fluorescent protein chromophore analogs.[6,7] Currently, the primary design scheme for fluorescent protein chromophore analogs involves modifying imidazolidinones with phenyl or aniline groups.[8,9] These compounds retain the fluorescence characteristics of fluorescent proteins and show great potential in fluorescence imaging and biological dyes. However, the emission wavelengths of these modulated FP chromophore analogs fall in the yellow or green spectral region, which causes photodamage to biological samples[10,11] and limits the depth of penetration in biological tissues.[12–15] Furthermore, the reported works on FP chromophore analogs mainly focus on applications such as viscosity probes,[16–18] DNA sensors,[19–21] and fluorescence imaging.[22] There has been less exploration in the construction of FP photosensitizers and photodynamic therapy (PDT). Compared to traditional photosensitizers such as BODIPY,[23,24] rhodamine,[25] and cyanine,[26] FP photosensitizers have better biocompatibility and lower dark toxicity that can facilitate access to biological tissues and reduce unnecessary damage to biological tissues.[27] However, current FP photosensitizers still suffer from low singlet oxygen ($^1O_2$) yields, short emission wavelengths, and a lack of organelle-targeting capabilities. Therefore, it is of great significance to develop novel near-infrared emitting FP chromophore analogs with organelle-targeting ability and to explore their applications in photodynamic therapy.

In our previous work, six-membered heterocyclic phenothiazines were introduced into imidazolidinones to obtain FP chromophore analogs (PFP) with good photophysical properties and singlet oxygen-generating ability.[5,27] Therefore, in this work, PFP was chosen as the basic structure, which was further modified to improve the emission wavelength and singlet oxygen yield, as well as to achieve good organelle targeting. As shown in Scheme 1, three novel fluorescent protein photosensitizers were constructed based on the *cis*-phenothiazine imidazolidinone structure through the Knoevenagel con-

School of Chemistry and Chemical Engineering, Southeast University, Nanjing 211189, China. E-mail: yingqian@seu.edu.cn

† Electronic supplementary information (ESI) available. See DOI: https://doi.org/10.1039/d3ob01966g

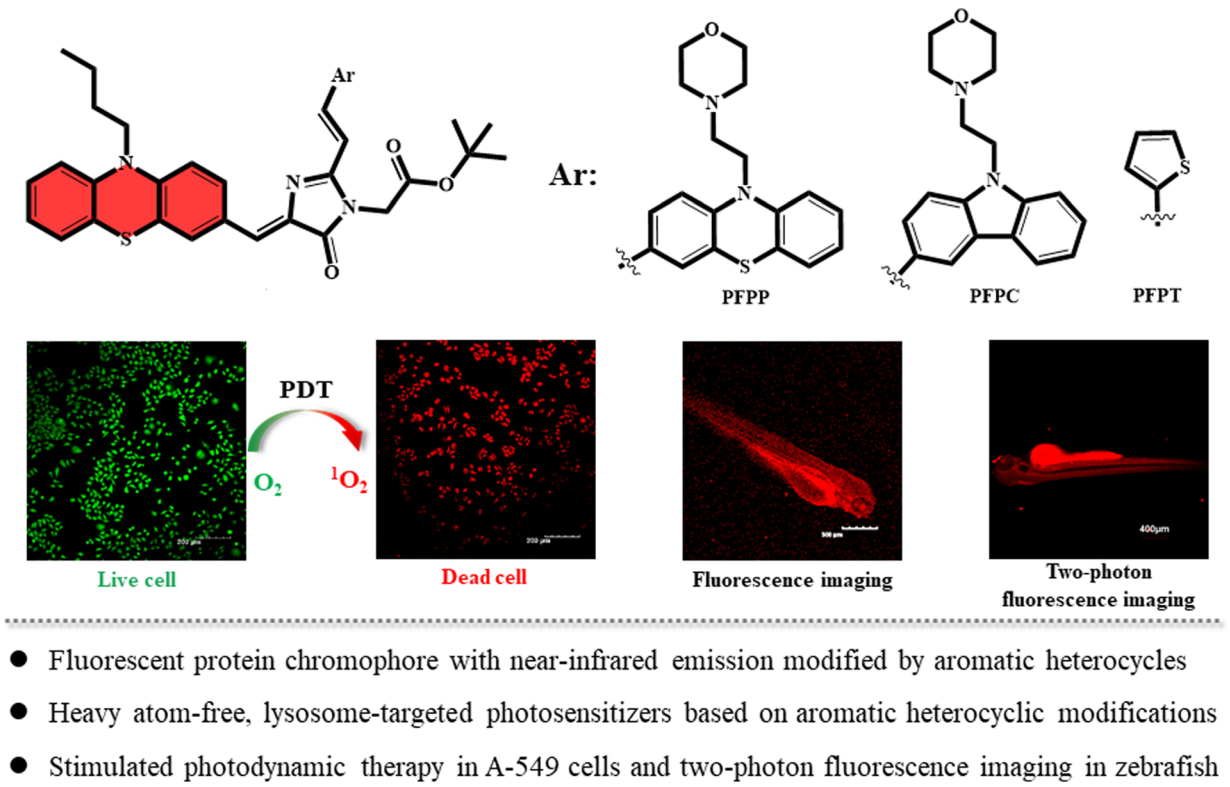

Scheme 1 Fluorescent protein chromophore analogs modified with five- and six-membered aromatic heterocycles for photodynamic therapy and two-photon fluorescence imaging.

densation with three heterocyclic compounds. The compound PFPP was obtained by linking PFP to morpholine-phenothiazine, PFPC was obtained by linking with morpholine-carbazole and PFPT was obtained by linking with thiophene. The three extended conjugated photosensitizers exhibited a significant improvement in the emission wavelength and photodynamic therapy-related parameters compared with the short-chain photosensitizer PFP. The effect of introducing heteroatoms (S and N) into the photosensitizers was briefly analyzed *via* theoretical calculations of excitation energies and singlet oxygen generation experiments. In the *in vitro* experiments, we evaluated the photodynamic therapy potential of the three photosensitizers by simulating photodynamic therapy experiments in A-549 cells and verified the lysosomal localization ability of photosensitizers PFPP and PFPC by organelle targeting experiments. Furthermore, two-photon fluorescence imaging experiments in zebrafish further support the potential value of these aryl heterocyclic constructed FP chromophore analogs for two-photon photodynamic therapy applications in biology.

2. Experimental

2.1 Materials and apparatus

All reagents and solvents were bought from Sinopharm Chemical Reagent Co., Ltd and Energy Chemical Corporation. All solvents were analytical grade and could be used directly without further purification. All biomaterials were purchased from Jiangsu Kaiji Biotechnology Co, Ltd. A-549 cells were used in this work, which were collected from the American Type Culture Collection (ATCC). The Bruker AVANCE III HD 600 NMR spectrometer was used to record ^{1}H NMR and ^{13}C NMR spectra with $CDCl_3$ as a solvent for the characterization of compounds. Agilent Technologies 6530 Accurate-Mass was used for recording mass spectra. The UV-Vis absorption spectrum was obtained using a Shimadzu UV-2600 ultraviolet–visible spectrophotometer, and the fluorescence spectrum was obtained using Horiba's FluoroMax-4 fluorescence spectrometer. The fluorescence quantum yield was determined using a C11347-11, Hamamatsu-absolute fluorescence quantum yield measuring meter. Cell biological imaging was performed under a confocal laser scanning microscope (FLUOVIEW FV3000, Olympus). Two-photon fluorescence imaging was performed under a confocal laser scanning microscope (FV3000, Olympus, laser: Ti:sapphire laser, pulse duration: 100 fs, and a focal plane of 800 nm: 40 mW cm^{-2}). The lamp used in the irradiation experiment was an LED (460 nm, 20 mW cm^{-2}). The detailed experimental procedures can be found in the ESI.†

2.2 Synthesis

Synthetic routes for 10-butyl-10*H*-phenothiazine-3-carbaldehyde (M_1), 10-(2-morpholinoethyl)-10*H*-phenothiazine-3-car-

baldehyde (M_2) and 9-(2-morpholinoethyl)-9*H*-carbazole-3-carbaldehyde (M_3) can be found in the ESI.† The photosensitizer PFP was synthesized based on published articles.[5,23]

Synthesis of PFPT. Thiophene-2-carbaldehyde (0.07 g, 0.62 mmol) was added to the toluene solution of PFP (0.20 g, 0.42 mmol), and piperidine (82.35 μL, 0.63 mmol) and acetic acid (62.61 μL, 0.84 mmol) were added for catalysis, heated to 110 °C and refluxed for 5 hours. After the reaction, the toluene solution was rotationally dried, separated, and purified by column chromatography to obtain an orange-red solid (ethyl acetate : petroleum ether = 1 : 6). Yield: 44%. ^{1}H NMR (600 MHz, chloroform-*d*) δ 8.18 (d, J = 15.4 Hz, 1H), 8.04 (s, 1H), 8.00 (d, J = 8.6 Hz, 1H), 7.39 (d, J = 5.0 Hz, 1H), 7.35 (d, J = 3.5 Hz, 1H), 7.16–7.11 (m, 2H), 7.04 (s, 1H), 6.96–6.92 (m, 2H), 6.90–6.85 (m, 2H), 6.39 (d, J = 15.4 Hz, 1H), 4.41 (s, 2H), 3.92–3.86 (m, 2H), 1.82 (m, 2H), 1.47 (s, 9H), 1.43 (d, J = 7.5 Hz, 2H), 0.96 (t, J = 7.4 Hz, 3H). ^{13}C NMR (151 MHz, chloroform-d) δ 170.04, 166.69, 157.39, 146.88, 144.05, 140.90, 137.44, 133.09, 132.43, 130.95, 130.85, 129.13, 128.38, 128.21, 127.45, 127.32, 126.62, 124.49, 124.04, 122.99, 115.57, 115.17, 111.72, 83.15, 47.52, 42.19, 28.93, 27.98, 20.13, 13.80. HRMS: $[C_{32}H_{34}N_3O_3S_2]^+$ calcd: 572.2036, obsd: 572.2061.

Synthesis of PFPP. M_2 (0.21 g, 0.62 mmol) was added to the toluene solution of PFP (0.20 g, 0.42 mmol), and piperidine (82.35 μL, 0.63 mmol) and acetic acid (62.61 μL, 0.84 mmol) were added for catalysis, heated to 110 °C and refluxed for 7 hours. After the reaction, the toluene solution was rotationally dried, separated, and purified by column chromatography to obtain a black-red solid (ethyl acetate : petroleum ether = 2 : 1). Yield: 47%. ^{1}H NMR (600 MHz, chloroform-d) δ 8.05 (s, 1H), 7.99 (d, J = 8.3 Hz, 1H), 7.95 (d, J = 15.6 Hz, 1H), 7.39 (d, J = 8.3 Hz, 1H), 7.36 (s, 1H), 7.19 (t, J = 7.6 Hz, 1H), 7.14 (dd, J = 13.3, 7.1 Hz, 3H), 7.03 (s, 1H), 6.96 (dq, J = 14.2, 7.4 Hz, 4H), 6.88 (dd, J = 8.2, 5.0 Hz, 2H), 6.47 (d, J = 15.6 Hz, 1H), 4.43 (s, 2H), 4.10 (s, 2H), 3.91–3.86 (m, 2H), 3.77 (s, 4H), 2.83 (s, 2H), 2.61 (s, 4H), 1.84–1.79 (m, 2H), 1.49 (m, 2H), 1.47 (s, 9H), 0.96 (t, J = 7.4 Hz, 3H). ^{13}C NMR (151 MHz, chloroform-d) δ 170.16, 166.79, 157.74, 146.80, 146.60, 144.95, 144.06, 132.39, 131.47, 130.91, 129.23, 129.15, 128.73, 127.60, 127.38, 126.55, 126.29, 126.01, 125.69, 125.11, 122.98, 122.75, 115.61, 115.55, 115.44, 83.14, 66.77, 55.77, 53.87, 53.82, 53.77, 47.51, 28.90, 28.01, 20.15, 13.84. HRMS: $[C_{46}H_{50}N_5O_4S_2]^+$ calcd: 800.3299, obsd: 800.3287.

Synthesis of PFPC. M_3 (0.19 g, 0.62 mmol) was added to the toluene solution of PFP (0.20 g, 0.42 mmol), and piperidine (82.35 μL, 0.63 mmol) and acetic acid (62.61 μL, 0.84 mmol) were added for catalysis, heated to 110 °C and refluxed for 7 hours. After the reaction, the toluene solution was rotationally dried, separated, and purified by column chromatography to obtain a black-red solid (ethyl acetate : petroleum ether = 3 : 1). Yield: 39%. ^{1}H NMR (600 MHz, chloroform-*d*) δ 8.31 (s, 1H), 8.26 (d, J = 15.6 Hz, 1H), 8.14 (d, J = 7.3 Hz, 1H), 8.07 (s, 1H), 8.03–7.99 (m, 1H), 7.75–7.71 (m, 1H), 7.51 (d, J = 8.0 Hz, 1H), 7.44 (d, J = 8.2 Hz, 2H), 7.31 (d, J = 7.5 Hz, 1H), 7.15 (t, J = 6.8 Hz, 2H), 7.02 (s, 1H), 6.94 (t, J = 7.4 Hz, 1H), 6.89 (dd, J = 11.5, 8.5 Hz, 2H), 6.64 (d, J = 15.6 Hz, 1H), 4.47 (s, 2H), 4.46 (d, J = 7.3 Hz, 2H), 3.92–3.87 (m, 2H), 3.70 (s, 4H), 2.78 (s, 2H), 2.55 (s, 4H), 1.83–1.79 (m, 2H), 1.50 (m, 2H), 1.48 (s, 9H), 0.97 (t, J = 7.4 Hz, 3H). ^{13}C NMR (151 MHz, chloroform-d) δ 170.48, 167.07, 157.64, 144.06, 141.54, 141.39, 141.14, 140.89, 140.49, 136.88, 130.67, 128.89, 128.75, 127.22, 126.81, 126.45, 126.20, 126.16, 125.74, 125.69, 123.53, 123.28, 122.89, 120.85, 120.62, 120.54, 119.94, 119.74, 109.96, 109.21, 108.95, 82.98, 77.27, 77.06, 76.85, 66.90, 56.67, 54.07, 42.47, 37.80, 28.04, 13.90. HRMS: $[C_{46}H_{50}N_5O_4S]^+$ calcd: 768.3579, obsd: 768.3576.

2.3 Theoretical calculation of photosensitizers

Molecular structure optimization and excited state energy calculations of photosensitizers were carried out using density functional theory.[28,29] Theoretical calculations were carried out using Gaussian 09 software, and the structures of the photosensitizers were first optimized using DFT//cam-B3LYP/6-31G(d), and the excited singlet and triplet state energies were calculated based on the optimization using TD-DFT//cam-B3LYP/6-31G(d,p)-D3.

2.4 Determination of singlet oxygen quantum yields and fluorescence quantum yields

1,3-diphenylisobenzofuran (DPBF) was used as a singlet oxygen scavenger to measure the quantum yield of singlet oxygen,[23,30] and $Ru(bpy)_3Cl_2$ was used as a standard (Φ_Δ = 87% methanol).[31] The yield of singlet oxygen mainly depends on the slope of DPBF absorbance decline and the irradiation time. The fluorescence quantum yield was determined using an absolute fluorescence quantum yield meter (Concentration: 1.0×10^{-5} M). Detailed steps can be found in the ESI.†

2.5 Singlet oxygen generation in A549 cells and zebrafish

Photosensitizer-mediated singlet oxygen production in A-549 cells and zebrafish was detected using the singlet oxygen indicator 2′,7′-dichlorodihydrofluorescein diacetate (DCFH-DA) according to the manual. Singlet oxygen production was analysed by analysing the fluorescence imaging results of cells and zebrafish under different experimental conditions. Detailed steps can be found in the ESI.†

2.6 Simulated photodynamic therapy in A-549 cells and fluorescence imaging in zebrafish

Cellular experiments include intracellular fluorescence imaging, singlet oxygen capture, MTT assays, AO/EB double staining experiments, and organelle localization experiments. Cellular fluorescence imaging experiments mainly detect photosensitizer uptake and assess biocompatibility. The singlet oxygen capture assay is used to detect the production of singlet oxygen under light radiation. The MTT assay is used to determine the darkness and phototoxicity of photosensitizers. The AO/EB (acridine orange/ethidium bromide) staining assay is used to determine apoptotic cell death. An organelle targeting assay was performed to determine the localization ability of photosensitizers. The zebrafish experiments include zebrafish fluorescence imaging experiments, two-photon fluorescence experiments, and singlet oxygen capture experiments.

The detailed procedure of these experiments can be found in the ESI.†

2.7 Ethical statement

All animal procedures were performed in accordance with the Guidelines for Care and Use of Laboratory Animals of Southeast University and approved by the Animal Ethics Committee of Southeast University.

3. Results and discussion

3.1 Fluorescent protein chromophores modified with five- and six-membered aromatic heterocycles

In this work, the phenyl structure of HBI was replaced with an electron-rich aryl heterocycle and further modified to extend the absorption and emission wavelengths of the dyes. As shown in Scheme 2, the parent compound PFP was obtained by linking heterocycle phenothiazine with imidazolinone, following the methodology outlined in our prior publication.[5] In the compound PFP skeleton, the phenothiazine and imidazolidinone rings are connected by a set of single–double bonds, and its conformation has both *-cis* and *-trans* possibilities due to intramolecular rotation.[4] The PFP single crystal structure was obtained by slow evaporation of the solvent to determine the *-cis* or *-trans* configuration. The data indicate that the cyclized building compound PFP is stable in the *cis*-configuration. Specific single-crystal data can be found in the ESI.†

Subsequently, the compound PFP was chosen as the basic structure for modification. Using piperidine/acetic acid as a catalyst, PFP was reacted with morpholino-phenothiazine *via* the Knoevenagel condensation reaction to obtain the target products PFPP. The photosensitizers PFPC and PFPT were obtained by linking the intermediate PFP with morpholino-carbazole and thiophene, respectively. All compounds were characterized by ^{1}H NMR, ^{13}C NMR, and high-resolution mass spectrometry and specific information could be found in the ESI.† The introduction of three aromatic heterocyclic rings can extend conjugation and increase the absorption and emission wavelengths of the dyes. The morpholine group on aromatic heterocycles can endow photosensitizers PFPP and PFPC with good lysosomal targeting ability. Furthermore, according to the El-Sayed rule,[32] the existence of a lone pair in heteroatoms such as S or N will promote a 1(n–π*) to 3(π–π*) transition in the excited states of photosensitizers, which could enhance the ISC process and improve singlet oxygen generation. The molecular structure optimization and excited state energy calculation of photosensitizers were carried out based on density functional theory (DFT) and time-dependent density functional theory (TD-DFT) to further briefly analyze the heterocyclic effect, and specific information can be found in the ESI.† The ΔE_{ST} between the singlet S_1 and triplet T_2 states of photosensitizer PFP is 0.36 eV and this energy gap is smaller than the energy region of ordinary photosensitizers, which can realize the ISC process. The ΔE_{ST} of the long-chain photosensitizers PFPAr were further reduced after the introduction of additional aromatic heterocycles, suggesting that the additional heteroatoms can further improve the ISC process. The energy gap of photosensitizer PFPP decreased the most and the ΔE_{ST} of PFPP reached 0.10 eV. We speculate that since

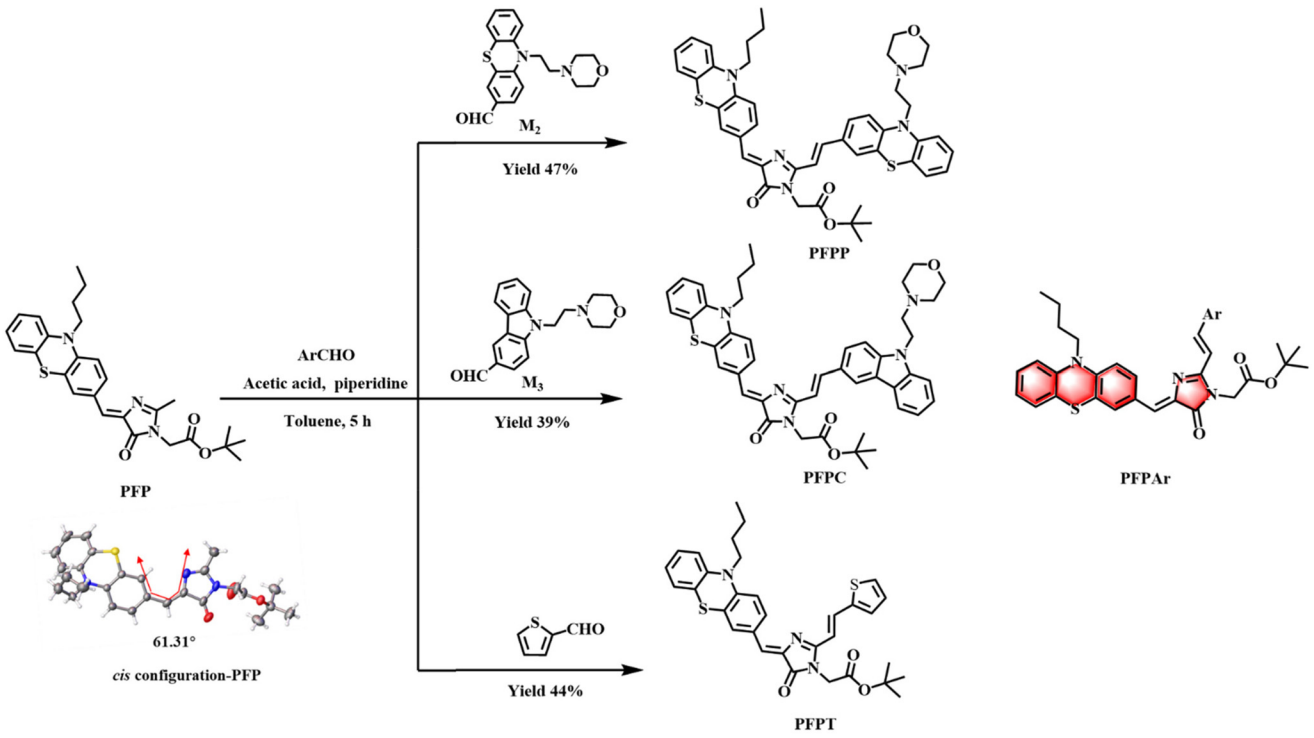

Scheme 2 The synthetic route of the photosensitizers.

PFPP contains two phenothiazines, more heteroatoms are introduced, reducing the energy gap and promoting ISC. The introduction of such five- or six-membered heterocycles at two sites of imidazolidinones has the potential for the development of fluorescent protein photosensitizers with higher emission wavelengths.

3.2 $^1O_2$ generation evaluation of fluorescent protein chromophore analog photosensitizers

The absorption and emission spectra of photosensitizers were analysed prior to the determination of singlet oxygen yields. As shown in Fig. 1(a), the maximum absorption peaks of the long-chain photosensitizers PFPT, PFPP, and PFPC were all at approximately 500 nm in methanol solvent. The absorption wavelengths were all red-shifted compared to the parent PFP (430 nm; ESI†) after the introduction of the aromatic heterocycles. Meanwhile, the molar extinction coefficients of the long-chain photosensitizers show an increasing trend and the enhancement was more obvious for the six-membered heterocyclic-modified photosensitizers PFPP and PFPC. As shown in Fig. 1(b), the fluorescence emission wavelengths of the three newly synthesised photosensitisers were also significantly larger relative to PFP (625 nm). Among them, the emission wavelengths of photosensitizers PFPP and PFPC were 701 nm and 710 nm, respectively, which reached the near-infrared band. The increase in emission wavelength can improve the penetration of the dyes into biological tissues and reduce damage to healthy tissues.[3] In addition, these heterocyclic-modified fluorescent protein dyes all have large Stokes shifts ($\Delta\lambda$), which avoid the overlap of absorption and emission spectra, thus effectively reducing the self-quenching phenomenon.[4] In short, the modification of the imidazolidinone structure using aromatic heterocycles can effectively increase the absorption and emission wavelengths of fluorescent protein dyes. The six-membered aryl heterocyclic phenothiazine and carbazole showed better results relative to thiophene.

Next, the singlet oxygen generation induced by photosensitizers under light irradiation was investigated using 1,3-diphenylisobenzofuran (DPBF), a typical singlet oxygen capture agent, whose absorption can be significantly quenched in the presence of singlet oxygen.[4] As shown in Fig. 2, when irradiated with a blue light source (460 nm), the absorption peak

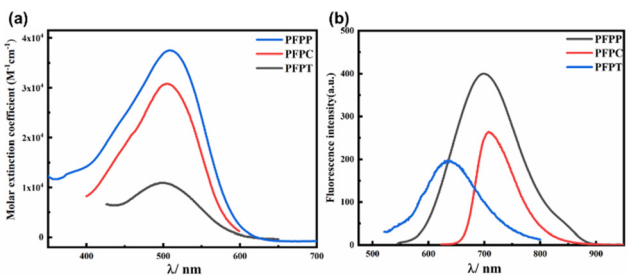

Fig. 1 (a) The UV-Vis absorption of photosensitizers PFPP, PFPC and PFPT. (b) The fluorescence emission spectroscopy of photosensitizers PFPP, PFPC and PFPT (1.0×10^{-5} M in methanol).

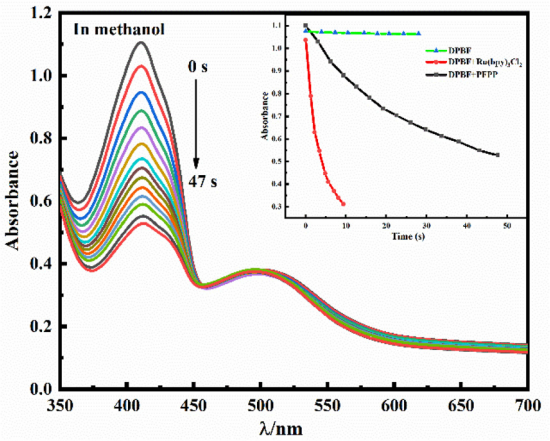

Fig. 2 The variation of absorbance of DPBF in methanol solution with the time of light exposure when PFPP is added as a photosensitizer (light: 460 nm, 20 mW cm^{-2}); the inset is the plot of change in the absorption of DPBF at 415 nm versus time under light irradiation. (DPBF, DPBF + PFPP, DPBF + $Ru(bpy)_3Cl_2$.)

at 415 nm of DPBF in PFPP solution reduced rapidly within 47 s, suggesting that singlet oxygen was produced efficiently by PFPP. The same experiment was performed for other photosensitizers under the same conditions, and the specific results can be found in the ESI.† The singlet oxygen yields (Φ_Δ) of PFPP, PFPC, and PFPT were calculated to be 23%, 17%, and 19%, respectively, by the relative method using $Ru(bpy)_3Cl_2$ as the reference (Φ_Δ = 0.87 in methanol). The Φ_Δ of the three newly synthesized photosensitizers show a slight improvement compared with the photosensitizer PFP (14%). This experimental result is consistent with the theoretical calculation, which is mainly because the introduction of heteroatoms reduces the ΔE_{ST} between the singlet and triplet states of the photosensitizers, thereby promoting the ISC process and increasing the Φ_Δ of the dyes. Among these photosensitizers, PFPP has the most enhanced singlet oxygen yield under the same conditions, which is consistent with the calculated ΔE_{ST} results (0.15 eV for PFPT, 0.12 eV for PFPC and 0.10 eV for PFPP). In short, the S or N atoms in the aromatic heterocycle can promote the ISC process and improve the photodynamic therapy parameters of the dyes. Among them, the electron-rich phenothiazine tricyclic structure introduced by PFPP has the most obvious enhancement effect. The measured photophysical property data and singlet oxygen yield data are listed in Table 1.

3.3 Two-photon fluorescence imaging and singlet oxygen detection in zebrafish

The photosensitizer PFPP was explored for fluorescence imaging applications in zebrafish due to its favourable fluorescence emission properties. We examined the fluorescence imaging of PFPP using confocal laser scanning microscopy (CLSM). The results shown in Fig. 3(a1) indicate remarkable red fluorescence in zebrafish after a period of incubation, indicating rapid internalisation of PFPP in zebrafish. Notably, as

Table 1 The basic optical spectral data, singlet oxygen efficiency and the fluorescence quantum yield of these photosensitizers in methanol

Compound	λ_{max}^{abs}/nm	ε_{max}/M^{-1} cm^{-1}	λ_{max}^{em}/nm	$\Delta\lambda$/cm^{-1}	Φ_Δ [a] (%)	Φ_F [b] (%)
PFP	430	9100	625	7255	14	0.11
PFPT	499	11 200	635	4292	19	0.17
PFPC	497	31 200	710	6036	17	0.21
PFPP	507	38 100	701	5458	23	0.39

[a] The singlet oxygen yield (Φ_Δ) was calculated by the relative method and the reference was $Ru(bpy)_3Cl_2$ (Φ_Δ = 87% methanol). [b] Fluorescence quantum yield (Φ_F) was absolute quantum yield (integrating sphere test; concentration: 1.0×10^{-5} M; solvent: methanol).

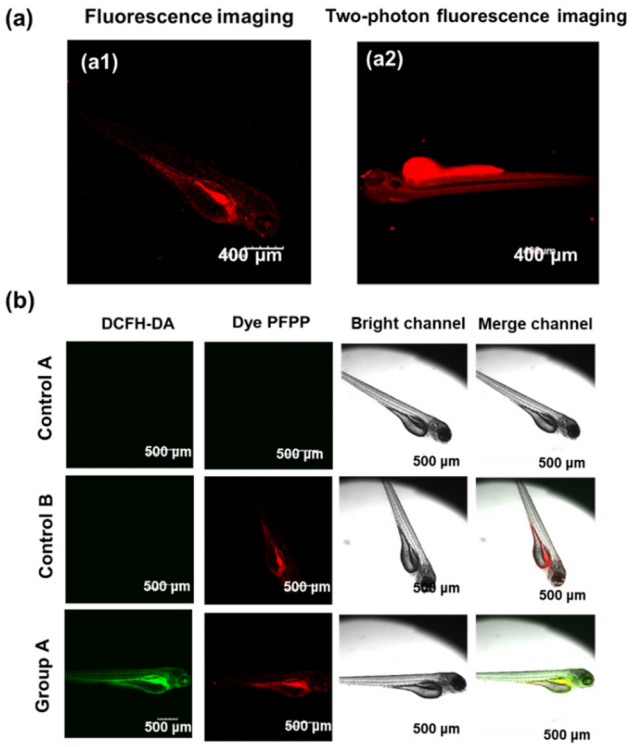

Fig. 3 (a1) The fluorescence imaging of zebrafish after co-incubation with the photosensitizer PFPP; (a2) The two-photon fluorescence imaging of zebrafish after co-incubation with the photosensitizer PFPP under 800 femtosecond excitation (concentration: 10^{-5} M). (b) ROS generation in zebrafish incubated with DCFH-DA + PFPP (5 μM) under different conditions: control group A: DCFH-DA (+), PFPP (–), light (+, 10 min); control group B: DCFH-DA (+), PFPP (+), light (–); group A DCFH-DA (+), PFPP (+), light (+, 10 min).

shown in Fig. 3(a2), clearer red fluorescence was detected in zebrafish after PFPP ingestion in the presence of an 800 nm femtosecond laser. The results indicate that PFPP has the capability of two-photon fluorescence imaging, enabling high-resolution fluorescence imaging of deep biological tissues, which offers the possibility of realising PDT in complex biology.[33,34]

Subsequently, 2′,7′-dichlorodihydrofluorescein diacetate (DCFH-DA) was used as a probe of reactive oxygen species to visualize singlet oxygen generation in zebrafish. The probe DCFH-DA can be hydrolysed by cytosolic esterases and emits green fluorescence after oxidation by reactive oxygen species.[3] Firstly, two sets of control experiments were performed. As shown in Fig. 3(b), the control A experiment was performed by incubating zebrafish with the dye DCFH-DA, followed by light irradiation, and showed no significant fluorescence in either channel. The control B experiment was performed by co-incubating zebrafish with the dyes DCFH-DA and PFPP without light irradiation. The image showed clear red fluorescence in the dye PFPP channel and negligible green fluorescence in the probe channel. Then, we proceeded to the experimental group where zebrafish were irradiated under light for 10 min after co-incubation with the dyes DCFH-DA and PFPP. As shown in Fig. 3(b), after 460 nm irradiation, strong green fluorescence was observed in zebrafish in the presence of PFPP, suggesting that abundant singlet oxygen were generated in zebrafish. These results clearly confirmed that PFPP has a strong capacity to generate intracellular singlet oxygen for PDT treatment.

3.4 Simulated photodynamic therapy in A-549 tumor cells

A-549 cells were chosen as the experimental system to further simulate *in vitro* photodynamic therapy experiments. Cellular toxicity experiments, cellular imaging experiments, singlet oxygen detection and live/dead cell double staining experiments were successively performed on photosensitisers. First, the dark toxicity and phototoxicity of photosensitizers were determined by the MTT method.[3] A-549 cells were cultured with a series of concentration gradients of PFPP and cell viability was tested in a dark environment and under light irradiation (460 nm), respectively. As shown in Fig. 4(a), prior to light irradiation, PFPP demonstrates negligible cytotoxicity, indicating excellent biocompatibility within the cellular

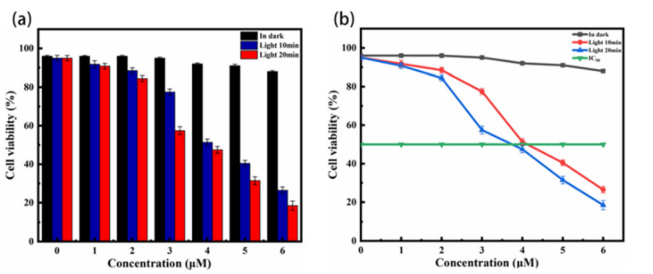

Fig. 4 (a) Cell Viability of A-549 cells incubated with PFPP in the dark and under 460 nm light irradiation for 10 and 20 min; (b) Cell growth curve of A-549 cells incubated with PFPP in the dark and under 460 nm light (20 mW cm^{-2}) irradiation for 10 and 20 min (the error is the result of three repetitions of the experiment).

environment. In contrast, it exhibited significant damage to A549 cells upon irradiation with 460 nm light (20 mW cm^{-2}). The cell viability was plotted as a line graph *versus* concentration as shown in Fig. 4(b). The curves showed that photosensitizer PFPP upon exposure to blue light decreased the viability of A-549 cells in a concentration-dependent manner and the half maximal inhibitory concentration (IC_{50}) value of PFPP was determined to be 4.12 μM after 10 min of light irradiation. The results above indicate that the photosensitizer PFPP has low dark toxicity but excellent phototoxicity.

Subsequently, cellular imaging of the photosensitizer PFPP was further investigated using cell confocal imaging. The photosensitiser PFPP was incubated with A-549 cells for 2 h, and then the cell culture dishes were washed twice with buffer (PBS) and observed with a laser scanning confocal microscope (CLSM). As shown in Fig. 5, cells impregnated with the dye PFPP showed bright red fluorescence. In addition, the cell state showed good shuttle shape morphology, indicating that the photosensitizer PFPP has low toxicity. Then, the singlet oxygen produced by the photosensitiser after light irradiation was detected in A-549 cells. As shown in Fig. 6, the results were the same as the previous experiments of the capture of reactive oxygen species in zebrafish. A-549 cells do not show green fluorescence without light exposure, and bright green fluorescence was observed after exposure to 460 nm light for 5 minutes. This result confirms that PFPP mediates the production of singlet oxygen in the cells.

To visually investigate the ability to induce tumor cell apoptosis, an acridine orange/ethidium bromide (AO/EB) double staining experiment was performed. AO would permeate through the cell membrane and enter the nucleus to insert into DNA. AO would emit green fluorescence after combination with DNA in the nucleus. On the other hand, the EB dye would only penetrate through impaired cell membranes and insert into nuclear DNA with red fluorescence emission.[4] Cells were incubated with photosensitizer PFPP (2 μM) for 2 h and then injected with AO/EB dyes (1 μM) for 10 minutes. As shown in Fig. 7, the control group experiment was performed in the dark, and the imaging cells showed uniform AO green fluorescence, without the unique red fluorescence of EB. In the experimental group A and group B, the red fluorescence of EB gradually increased and the green fluorescence of AO gradually weakened after 460 nm lamp irradiation for a while. The cells were almost completely apoptotic after 15 min of irradiation. This result demonstrates that PFPP dyes have the potential to be photosensitizers. In short, the above results indicate that PFPP exhibits good biocompatibility and causes little damage to cells under dark conditions. Meanwhile, a low dose of photosensitizer PFPP can effectively eliminate A-549 cells under light irradiation.

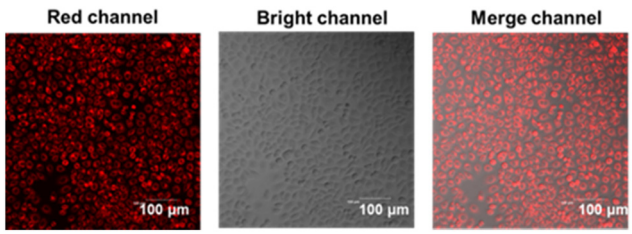

Fig. 5 The fluorescence imaging of PFPP in A-549 cells (2 μM); red channel: the fluorescence channel that captures the dye's emission band; bright channel: the laser beam creates a bright field of light to detect the shape of the object channel; merge channel: two channels of superimposed images.

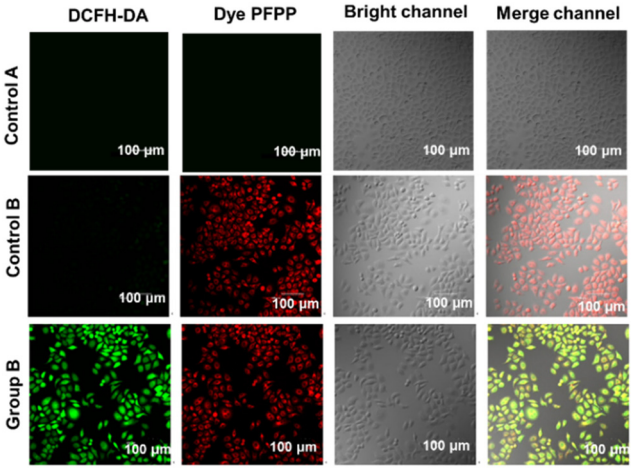

Fig. 6 ROS generation in A-549 cells incubated with DCFH-DA + PFPP (2 μM) under different conditions: control group A: DCFH-DA (+), PFPP (–), light (+, 5 min); control group B: DCFH-DA (+), PFPP (+), light (–); group A DCFH-DA (+), PFPP (+), light (+, 5 min). λ_{ex} = 488 nm, λ_{em} = 488–520 nm. Green channel: the fluorescence channel for capturing the emission band of the dye DCFH-DA; red channel: the fluorescence channel that captures the dye's emission band.

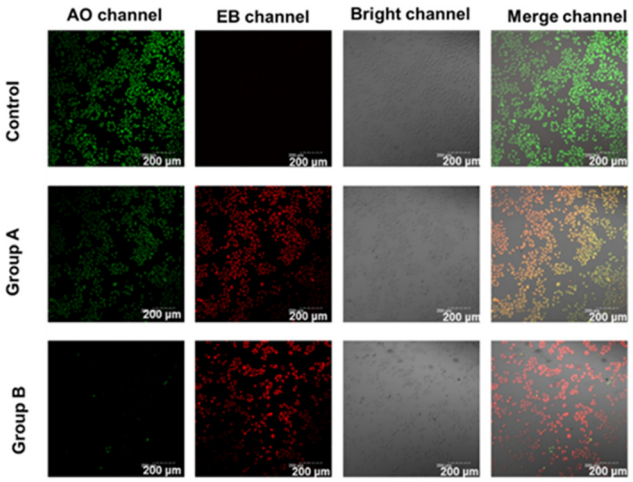

Fig. 7 Dead/live cell staining assay of A-549 cells incubated with PFPP at different lighting times (Control: 0 min; group A: 5 min; group B: 15 min, light: 460 nm, 20 mW cm^{-2}). AO channel: the fluorescence channel for capturing the emission band of the dye AO; EB channel: the fluorescence channel for capturing the emission band of the dye EB.

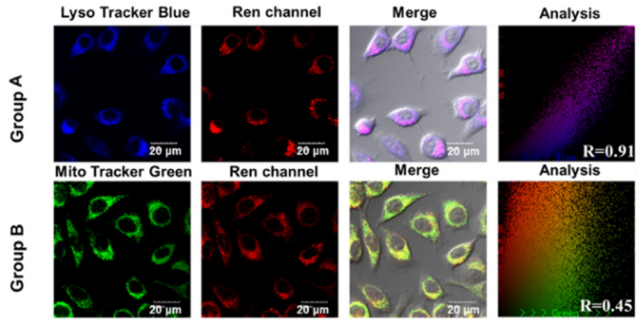

Fig. 8 Photosensitizer PFPP co-localization imaging in A-549 cells. Group A: lysosomal targeting experiment. Group B: mitochondrial targeting experiment.

3.5 Co-localization of fluorescent protein photosensitizers in subcellular organelles

During photodynamic therapy, the effectiveness of photoconductive therapy is greatly limited by the short lifetime (~100 ns) and limited diffusion (10–100 nm) of singlet oxygen.[35] Compared to photodynamic therapy at the tissue and cellular levels, organelle-targeted photodynamic therapy can further improve the precise killing efficiency of diseased cells.[36] The localization assay was performed in A-549 cells using commercially available trackers Lyso-Tracker Blue and Mito-Tracker Green to study the organelle localisation capacity of PFPP and PFPC. As shown in Fig. 8, photosensitizer PFPP (2 μM) and Lyso-Tracker Green (0.5 μM) were incubated with A-549 cells for 10 min. The blue fluorescence displayed by Lyso-Tracker Blue overlaps well with the red fluorescence displayed by PFPP. The image pixels were analysed by using the software and the Pearson correlation coefficient was calculated to be 0.91, indicating good localisation of the photosensitiser PFPP in the lysosomes of the cells. The same experiment was performed under the same conditions using the dye Mito-Tracker Green. The red fluorescence of the dye itself only partially overlapped with the green fluorescence of mitochondria, and its Pearson correlation coefficient is 0.45. This shows that the photosensitizer PFPP is preferentially located in lysosomes and the excellent co-localization ability of lysosomes is mainly due to the morpholine group favoring the acidic environment of the lysosomes.[4] The same experiments were performed on the dye PFPC, and the specific data can be found in the ESI.†

In short, the combination of laboratory experiments, zebrafish imaging experiments and A-549 cell-mimicking PDT experiments demonstrates that the photosensitizers PFPAr have great potential for application in photodynamic therapy in the biological near-infrared window and also proves that the rational introduction of heterocyclic rings is an effective way to improve the performance of the material.

4. Conclusion

In summary, three fluorescent protein photosensitisers PFPAr (PFPP, PFPC, and PFPT) were synthesised by modifying the photosensitiser PFP with five- or six-membered aromatic heterocycles. With the introduction of the aromatic heterocycles, the absorption and emission wavelengths of the synthesized photosensitizers were red-shifted and the emission wavelengths of PFPP and PFPC reached the near-infrared region at 701 nm and 710 nm, respectively. In addition, the determination of singlet oxygen yield and theoretical calculation indicate that the introduction of heterocyclic rings containing S or N promotes the ISC process and slightly improves singlet oxygen yield. In biological applications, all the three photosensitizers have good biocompatibility and can be taken up by cells within a short period of time. The results of the MTT assay showed that new photosensitizers have low darkness and excellent phototoxicity. The reactive oxygen imaging experiments and AO/EB double staining assay indicate that PFPAr can generate singlet oxygen to eliminate A-549 tumor cells effectively with photoexcitation of 460 nm blue light. Moreover, the morpholine structure in the dyes confers lysosomal targeting ability to the photosensitisers PFPP and PFPC, enabling them to label the lysosomes of tumour cells. Remarkably, these heterocyclically modified fluorescent protein photosensitisers are capable of two-photon fluorescence imaging under 800 nm femtosecond excitation. The rational introduction of aromatic heterocycles into photosensitizers is an effective way to improve the PDT parameters of fluorescent protein photosensitizers and the ensuing nonlinear optical properties make it promising for application in further two-photon photodynamic therapy.

Author contributions

Li Weilong: synthesis and testing of compounds and writing of the first draft; Feng Wan: synthesis and revision of the first draft; Liu Badi: theoretical calculation test; Qian Ying: fund acquisition, concept formation, writing review, and editing.

Conflicts of interest

There are no conflicts to declare.

Acknowledgements

We thank the financial support from the Fundamental Research Funds for the National Natural Science Foundation of China (No. 62075039).

References

1 Y. Liu, C. H. Wolstenholme, G. C. Carter, H. Liu, H. Hu, L. S. Grainger, K. Miao, M. Fares, C. A. Hoelzel, H. P. Yennawar, G. Ning, M. Du, L. Bai, X. Li and X. Zhang, *J. Am. Chem. Soc.*, 2018, **140**, 7381–7384.

2 A. Svendsen, H. V. Kiefer, H. B. Pedersen, A. V. Bochenkova and L. H. Andersen, *J. Am. Chem. Soc.*, 2017, **139**, 8766–8771.
3 W. Feng, W. Li and Y. Qian, *Dyes Pigm.*, 2023, **220**, 111714.
4 W. Li, W. Feng, B. Liu and Y. Qian, *J. Photochem. Photobiol., A*, 2023, **445**, 115045.
5 W. Xiang, B. Liu and Y. Qian, *Dyes Pigm.*, 2022, **205**, 110524.
6 W. Fan, H. Deng, L. Zhu, C. Tu, Y. Su, L. Shi, J. Yang, L. Zhou, L. Xu and X. Zhu, *Biomater. Sci.*, 2019, **7**, 2421–2429.
7 X. Zhi, W. Xiang and Y. Qian, *J. Lumin.*, 2021, **240**, 118424.
8 L. Cai, H. Li, X. Yu, L. Wu, X. Wei, T. D. James and C. Huang, *ACS Appl. Bio Mater.*, 2021, **4**, 2128–2134.
9 H. Leng, Y. Wang, J. Wang, H. Sun, A. Sun, M. Pistolozzi, L. Zhang and J. Yan, *Anal. Chem.*, 2022, **94**, 1999–2006.
10 F. Bolze, S. Jenni, A. Sour and V. Heitz, *Chem. Commun.*, 2017, **53**, 12857–12877.
11 L. Wu, J. Liu, P. Li, B. Tang and T. D. James, *Chem. Soc. Rev.*, 2021, **50**, 702–734.
12 R. F. Avena, L. Qiao, Y. Fujii, K. Otomo, H. Ishii, T. Suzuki, H. Tsujino, T. Uno, Y. Tsutsumi, Y. Kawashima, T. Takagi, K. Murai, T. Nemoto and M. Arisawa, *ACS Omega*, 2020, **5**, 2473–2479.
13 M. Drobizhev, R. S. Molina and J. Franklin, *Int. J. Mol. Sci.*, 2022, **23**, 770.
14 H. L. Ng and M. Z. Lin, *Curr. Opin. Struct. Biol.*, 2016, **39**, 124–133.
15 D. M. Shcherbakova, O. V. Stepanenko, K. K. Turoverov and V. V. Verkhusha, *Trends Biotechnol.*, 2018, **36**, 1230–1243.
16 L. Liu, W. Jin, Y. Huang, J. Dai, X. Zheng, Y. Liu, M. Ju and B. Shen, *Sens. Actuators, B*, 2022, **353**, 131098.
17 H. Sun, H.-x. Leng, J.-s. Liu, G. Roy, J.-w. Yan and L. Zhang, *Sens. Actuators, B*, 2020, **305**, 127509.
18 X. Zhi, B. Shen and Y. Qian, *New J. Chem.*, 2020, **44**, 8823–8832.
19 C. E. Copeland, J. Kim, P. L. Copeland, C. J. Heitmeier and Y. C. Kwon, *ACS Synth. Biol.*, 2022, **11**, 2800–2810.
20 M. Fujita, M. Goto, M. Tanaka and W. Yoshida, *Anal. Methods*, 2023, **15**, 2294–2299.
21 X. Zhi and Y. Qian, *Talanta*, 2021, **222**, 121503.
22 L. Hauke, S. Isbaner, A. Ghosh, I. Guido, L. Turco, A. I. Chizhik, I. Gregor, N. Karedla, F. Rehfeldt and J. Enderlein, *ACS Nano*, 2023, **17**, 8242–8251.
23 M. Liu, C. Wang and Y. Qian, *New J. Chem.*, 2021, **45**, 18082–18089.
24 L. Wang and Y. Qian, *Dyes Pigm.*, 2021, **195**, 109711.
25 H. Shigemitsu, K. Sato, S. Hagio, Y. Tani, T. Mori, K. Ohkubo, Y. Osakada, M. Fujitsuka and T. Kida, *ACS Appl. Nano Mater.*, 2022, **5**, 14954–14960.
26 H. Ma, Y. Lu, Z. Huang, S. Long, J. Cao, Z. Zhang, X. Zhou, C. Shi, W. Sun, J. Du, J. Fan and X. Peng, *J. Am. Chem. Soc.*, 2022, **144**(8), 3477–3486.
27 W. Xiang, X. Zhi, L. Zhang and Y. Qian, *Chin. J. Org. Chem.*, 2021, **41**, 3578–3584.
28 M. Li, R. Tian, J. Fan, J. Du, S. Long and X. Peng, *Dyes Pigm.*, 2017, **147**, 99–105.
29 L. Wang and Y. Qian, *Biomater. Sci.*, 2023, **11**, 1459–1469.
30 L. Huang, Z. Li, Y. Zhao, Y. Zhang, S. Wu, J. Zhao and G. Han, *J. Am. Chem. Soc.*, 2016, **138**, 14586–14591.
31 C. Tanielian, C. Wolff and M. Esch, *J. Phys. Chem.*, 1996, **100**, 6555–6560.
32 X. Liu, L. Yang, X. Li, L. Zhao, S. Wang, Z. H. Lu, J. Ding and L. Wang, *Angew. Chem., Int. Ed.*, 2021, **60**, 2455–2463.
33 Z. Wu, M. Liu, Z. Liu and Y. Tian, *J. Am. Chem. Soc.*, 2020, **142**, 7532–7541.
34 L. Xu, J. Zhang, L. Yin, X. Long, W. Zhang and Q. Zhang, *J. Mater. Chem. C*, 2020, **8**, 6342–6349.
35 M. Li, R. Tian, J. Fan, J. Du, S. Long and X. Peng, *Dyes Pigm.*, 2017, **147**, 99–105.
36 Y. Hu, S.-Y. Yin, Z. Li, W. Qi, Y. Chen and J. Li, *Chem. Commun.*, 2022, **58**, 13143–13146.